

Lane-Deviation Penalty for Autonomous Avoidance Maneuvers

Pavel Anistratov, Björn Olofsson, & Lars Nielsen

Division of Vehicular Systems, Department of Electrical Engineering

Linköping University, Sweden

E-mail: pavel.anistratov@liu.se

Topic: Vehicle Dynamics and Chassis Control

A formulation of an offline motion-planning method for avoidance maneuvers based on a lane-deviation penalty function is proposed, which aims to decrease the risk of a collision by minimizing the time when a vehicle is outside of its own driving lane in the case of avoidance maneuvers. The penalty function is based on a logistic function. The method is illustrated by computing optimal maneuvers for a double lane-change scenario. The comparison with minimum-time and squared-error norm maneuvers shows that the use of the considered penalty function requires fewer constraints and decreases the time that the vehicle stays in the opposing lane. The same objective function, whose parameters are dependent on the road configuration, allows to obtain trajectories for varying obstacles with many similarities between trajectories. This property is desirable for reuse of the resulting maneuvers in an online motion planner.

1 INTRODUCTION

Development of (semi-)autonomous vehicles allows utilization of new optimal driving approaches that could increase vehicle safety by combining optimal all-wheel braking and steering in at-the-limit operation. Sophisticated offline methods are available to obtain an accurate motion plan in time-critical situations using nonlinear optimization techniques together with realistic tire and chassis models, see, *e.g.*, [1]. Available vehicle and tire models allow studying aggressive vehicle maneuvers, for example a pendulum-turn maneuver, with results matching data obtained from a racing car [2].

Results from offline motion-planning studies of evasive maneuvers have been used, for example, to develop a better closed-loop longitudinal controller for online use [3]. The development of autonomous vehicles drives the interest for online motion methods that are feasible to use onboard, but still capture desired properties of the complex vehicle dynamics.

An approach for making complex vehicle models tractable for online motion planning is to use a maneuver-based planner, where a database of maneuvers created offline is used to obtain a motion plan. Such an approach is in [4] shown to work for motion planning of a small aerobatic helicopter. The same general approach can also allow to design a motion planner for time-critical situations of ground vehicles. An example of such a situation is a double lane-change maneuver. That maneuver is considered in this paper and is inspired by the ISO double lane-change test [5], which is also known in Scandinavian countries as the “moose test” (*i.e.*, the investigation of an evasive maneuver for a moose on the road, see Figure 1).

To obtain maneuvers for a database, optimization techniques to find optimal maneuvers for the considered setup can be used. For that purpose, an objective function should be selected. Common ways to obtain at-the-limit maneuvers are to minimize the final time of the maneuver [1] or to split the maneuver into several segments with different optimization criteria [6]. Such approaches often lead to extreme values of the vehicle state variables (*e.g.*, high vehicle sideslip values and maximum utilization

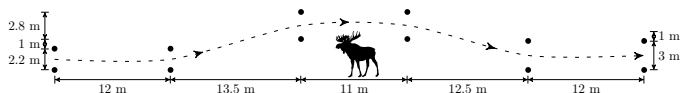


Figure 1: Sketch of the double lane-change maneuver with a potential obstacle.

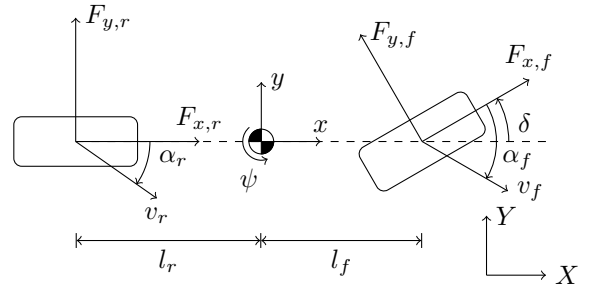


Figure 2: The single-track model.

of the tire forces), without necessarily taking a passenger’s perspective into account. It is dangerous for the vehicle to be in the opposing lane, but it is safe to drive in the original lane again after the obstacle. To capture this idea, we use a lane-deviation penalty (LDP) objective function to avoid obstacles, which penalizes being outside of the own driving lane.

2 MODELING

The single-track model (see, *e.g.*, [7]) is used to describe the vehicle dynamics with the following equations:

$$\dot{v}_x - v_y \dot{\psi} = \frac{1}{m} (F_{x,f} \cos(\delta) - F_{y,f} \sin(\delta)),$$

$$\dot{v}_y + v_x \dot{\psi} = \frac{1}{m} (F_{y,f} \cos(\delta) + F_{x,f} \sin(\delta)),$$

$$I_Z \ddot{\psi} = l_f F_{y,r} \cos(\delta) - l_r F_{y,r} + l_f F_{x,f} \sin(\delta),$$

$$\dot{v}_x - v_y \dot{\psi} = \frac{F_X}{m}, \dot{v}_y + v_x \dot{\psi} = \frac{F_Y}{m}, I_Z \ddot{\psi} = M_Z,$$

where v_x , v_y are the longitudinal and lateral velocities at the center-of-gravity, $\dot{\psi}$ is the yaw rate, δ is the steering angle, $F_{x,i}$, $F_{y,i}$, $i \in \{f, r\}$, are the longitudinal and lateral forces for the front and the rear wheels, respectively, m is the vehicle mass, l_f , l_r are defined in Figure 2, I_Z is the vehicle chassis inertia in the yaw direction, and F_X , F_Y , and M_Z are the global forces.

The slip angles α_i and slip ratios κ_i are defined as in [8]:

$$\dot{\alpha}_i \frac{\sigma}{v_{x,i}} + \alpha_i = -\arctan\left(\frac{v_{y,i}}{v_{x,i}}\right), \kappa_i = \frac{R_{\omega} \omega_i - v_{x,i}}{v_{x,i}}, i \in \{f, r\},$$

where σ is the relaxation length, R_ω is the wheel radius, ω_i is wheel angular velocity for wheel i , $v_{x,i}$ and $v_{y,i}$ are the longitudinal and lateral wheel velocities for wheel i , with respect to its own coordinate system.

The wheel dynamics are given by (see [1])

$$T_i - I_\omega \dot{\omega}_i - F_{x,i} R_\omega = 0, \quad i \in \{f, r\},$$

where T_i is the driving/braking torque and I_ω is the wheel inertia.

The nominal tire forces $F_{x0,i}$ and $F_{y0,i}$ are computed using the Pacejka Magic Formula model [8]:

$$\begin{aligned} F_{x0,i} &= \mu_{x,i} F_{z,i} \sin(C_{x,i} \arctan(B_{x,i} \kappa_i \\ &\quad - E_{x,i}(B_{x,i} \kappa_i - \arctan(B_{x,i} \kappa_i)))), \\ F_{y0,i} &= \mu_{y,i} F_{z,i} \sin(C_{y,i} \arctan(B_{y,i} \alpha_i \\ &\quad - E_{y,i}(B_{y,i} \alpha_i - \arctan(B_{y,i} \alpha_i))), \end{aligned}$$

for each wheel $i \in \{f, r\}$, where μ_x and μ_y are the friction coefficients and B , C , and E are model parameters.

The forces under combined longitudinal and lateral slip are calculated using weighting functions $G_{x\alpha,i}$ and $G_{y\kappa,i}$ [8] for the longitudinal and the lateral directions:

$$\begin{aligned} H_{x\alpha,i} &= B_{x1,i} \cos(\arctan(B_{x2,i} \kappa_i)), \\ G_{y\alpha,i} &= \cos(C_{x\alpha,i} \arctan(H_{x\alpha,i} \alpha_i)), \\ F_{x,i} &= F_{x0,i} G_{x\alpha,i}, \\ H_{y\kappa,i} &= B_{y1,i} \cos(\arctan(B_{y2,i} \alpha_i)), \\ G_{y\kappa,i} &= \cos(C_{y\kappa,i} \arctan(H_{y\kappa,i} \kappa_i)), \\ F_{y,i} &= F_{y0,i} G_{y\kappa,i}, \quad i \in \{f, r\}, \end{aligned}$$

where B and C are model parameters.

The models were implemented using the Modelica language [9], and numerical optimizations were performed using the platform JModelica.org and the Ipopt software package for nonlinear optimization [10], together with the MA57 linear solver [11]. Further details on the implementation and optimization of the models are available in [1].

3 OPTIMAL CONTROL PROBLEM

This section describes how the motion-planning problem of the double lane-change maneuver is represented as an optimal control problem. The particular choice of the parameters and prerequisites for the problem is given.

3.1 Formulation of the Optimal Control Problem

To represent the objective function and road constraints in the optimization, a function $\tilde{H}_{a_o}^{a_r}(a)$ is used that represents a smooth approximation of the Heaviside step function with an offset a_o and a rising distance a_r , which is also known as the logistic function (see Figure 3):

$$\tilde{H}_{a_o}^{a_r}(a) = \frac{1}{2} + \frac{1}{2} \tanh\left(\frac{\pi}{a_r}(a - a_o)\right). \quad (1)$$

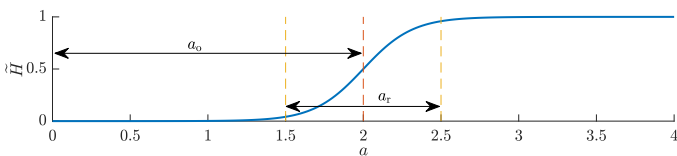


Figure 3: Example of the \tilde{H} function for $a_o = 2$ and $a_r = 1$.

To obtain optimal trajectories with the considered penalty function, the motion-planning problem for the studied double lane-change maneuver is formulated as an optimization problem in the following way:

$$\min. \quad \int_0^{t_f} \tilde{H}_{Y_o}^{Y_r}(Y(t)) dt \quad (2)$$

$$\text{s.t.} \quad T_{i,\min} \leq T_i \leq T_{i,\max}, \quad |\dot{T}_i| \leq \dot{T}_{i,\max}, \quad i \in \{f, r\},$$

$$|\delta| \leq \delta_{\max}, \quad |\dot{\delta}| \leq \dot{\delta}_{\max}, \quad \sqrt{v_x^2 + v_y^2} < v_0, \quad (3)$$

$$X(0) = X_0, \quad Y(0) = Y_0, \quad \psi(0) = 0, \quad \psi(t_f) = 0,$$

$$v_X(0) = v_0, \quad v_Y(0) = 0, \quad X(t_f) = X_{t_f}, \quad Y(t_f) \leq Y_{t_f},$$

$$Y_{bb}(X(t)) \leq Y(t), \quad \dot{\mathbf{x}} = G(\mathbf{x}, \mathbf{u}), \quad h(\mathbf{x}, \mathbf{u}) = 0.$$

where Y_o and Y_r define the LDP and t_f is the total time of the maneuver, which is unknown *a priori*. The projection on the Y -axis of the LDP used in the objective function is shown with the purple curve in, for example, Figures 4 and 5. The vehicle dynamics, $\dot{\mathbf{x}} = G(\mathbf{x}, \mathbf{u})$, is formulated for the states \mathbf{x} and inputs \mathbf{u} :

$$\mathbf{x} = \{X, Y, \psi, \dot{\psi}, T_f, T_r, \delta, v_x, v_y, \omega_f, \omega_r, \alpha_f, \alpha_r\},$$

$$\mathbf{u} = \{\dot{\delta}, \dot{T}_f, \dot{T}_r\}.$$

The tire dynamics is formulated as $h(\mathbf{x}, \mathbf{u}) = 0$. The wheel driving/braking torque $T_i, i \in \{f, r\}$, and the steering angle δ are bounded as well as their first derivatives. The drivable area is bounded below for Y (the position of the center-of-mass of the vehicle) by the function $Y_{bb}(X(t))$ representing the bottom boundary. The vehicle starts the movement at the point (X_0, Y_0) with the velocity v_0 and zero heading ($\psi = 0$). The final point is defined to be at X_{t_f} with zero heading and below Y_{t_f} , where the last condition is imposed, such that the vehicle ends on an appropriate lane position.

The common way to navigate a double lane-change maneuver (as it is also described in the standard [5]) is to only use braking with the throttle released, so the maneuver is performed without an increase in the velocity. The analysis in [3] showed the importance of speed in some avoidance scenarios. In this paper, the default version of the maneuver that we consider allows positive acceleration, but the velocity is upper bounded by the initial velocity v_0 .

The bottom boundary of the drivable area $Y_{bb}(X(t))$ is defined as:

$$Y_{bb}(X(t)) = Y_{bbp}(\tilde{H}_{X_{ou}}^{X_r}(X(t)) - \tilde{H}_{X_{od}}^{X_r}(X(t))), \quad (4)$$

where X_{ou} and X_{od} define points on the X -axis where the bottom boundary goes up and down in the Y -direction, respectively, X_r determines the sharpness of the transition, and Y_{bbp} defines the peak value for the bottom boundary.

3.2 Optimization Prerequisites

The maximum allowed wheel angle δ_{\max} and wheel-angle change rate $\dot{\delta}_{\max}$ are set to 0.5 rad and 1 rad/s, respectively.

The vehicle starts at the point $X_0 = 0$ m and $Y_0 = 1$ m in XY coordinates with the default initial velocity $v_0 = 70$ km/h along the X -axis and zero velocity along the Y -axis. The vehicle moves in the positive direction of X . The final point is at $X_{t_f} = 100$ m and below $Y_{t_f} = Y_0$.

The final point X_{t_f} is set to 100 m, which is more than defined by the maneuver illustrated in Figure 1, where the maneuver is shown with a total length along the X direction of 61 m. Additional distance is added to verify that the vehicle goes back to the own lane and could follow it. Since the last meters of the maneuver, usually, are less critical from the lane-change perspective, most further plots are for illustration purposes presented in

Table 1: Chassis and wheel parameters. Adopted from [1] for the single-track model.

Notation	Value	Unit	Notation	Value	Unit
l_f	1.3	m	R_ω	0.3	m
l_r	1.5	m	I_ω	4.0	kgm ²
m	2100	kg	σ	0.3	m
I_Z	3900	kgm ²	g	9.82	ms ⁻²

Table 2: Tire-model parameters for dry asphalt from [8].

Notation	Front	Rear	Notation	Front	Rear
μ_x	1.2	1.2	E_y	-1.21	-1.11
B_x	11.7	11.1	B_{x1}	12.4	12.4
C_x	1.69	1.69	B_{x2}	-10.8	-10.8
E_x	0.377	0.362	$C_{x\alpha}$	1.09	1.09
μ_y	0.935	0.961	B_{y1}	6.46	6.46
B_y	8.86	9.3	B_{y2}	4.20	4.20
C_y	1.19	1.19	$C_{y\kappa}$	1.08	1.08

a truncated form to highlight the most interesting parts of the maneuver.

The lower and upper constraints on the torque inputs are chosen as:

$$T_{i,\min} = -\mu_{x,i} R_\omega m g, \quad i \in \{f, r\},$$

$$T_{r,\max} = \mu_{x,r} R_\omega F_{z0,r}, \quad T_{f,\max} = 0,$$

where the nominal load $F_{z0,r}$ is given by $mg l_r / (l_r + l_f)$ and g is the gravitational acceleration constant. The constraint on the derivate of the torque inputs is chosen as:

$$\dot{T}_{i,\max} = 2.5 \mu_{x,i} R_\omega, \quad i \in \{f, r\}.$$

The parameters for the objective function (2) are set to $Y_o = 2$ m and $Y_r = 2$ m, and the parameters defining the boundaries of the drivable area are set to $X_{ou} = 23.5$ m, $X_{od} = 36.5$ m, $X_r = 2$ m, and $Y_{bbp} = 4$ m.

The constraints for the vehicle position are imposed on the center-of-mass. All boundaries of the drivable area are adjusted based on the consideration that the full vehicle chassis in the middle of the lane has unoccupied space of 1 m on both sides, making the width of the drivable lane 2 m in total.

The values for the chassis and wheel parameters are provided in Table 1. The values of the tire parameters are presented in Table 2.

4 PARAMETER VARIATIONS

Motivated by the desire to create a sparse data set of maneuvers, we are interested in studying changes in the resulting trajectories for different parameter variations. In this section, we study variations in the problem for the obstacle width and length, for the distance to the obstacle, as well as for the initial velocity of the vehicle and influence of steering dynamics.

4.1 Obstacle Width

Variations in the obstacle width w , *i.e.*, the road width occupied by the obstacle along the Y -direction, are studied. The obtained paths are shown in Figures 4. The same LDP objective (2) is used for all optimizations with parameters that are motivated by the road width, but the bottom drivable area is modified, namely Y_{bbp} in (4). The shapes of the XY -paths are very similar when comparing different widths of the obstacle. The increase in the obstacle width shows an expected increase in the extreme values for the vehicle orientation ψ .

In Figure 4, the velocity profiles for obstacles up to 4.5 m width have almost the same shape for the major part of the maneuver. For wider obstacles, the velocity profiles are no longer the same, but they change in a predictable manner. For the obstacle width $w = 2$ m, which allows the vehicle to perform a maneuver without leaving its own lane, the optimal steering strategy

differs for the middle part of the maneuver (δ in Figure 4), because the LDP penalty around $Y = 2$ m has a nonzero gradient, so steering toward the obstacle is optimal.

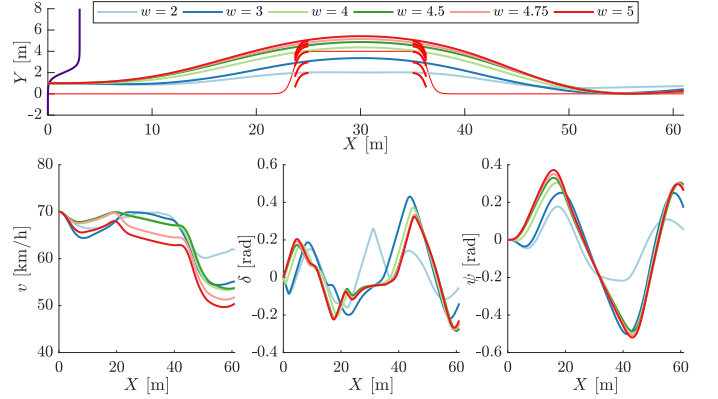


Figure 4: Paths and selected vehicle variables found for different obstacle widths (in meters), with the initial velocity $v_0 = 70$ km/h. The same LDP objective, but different Y_{bbp} is used. Red arcs show the top boundaries of the obstacle for different obstacle widths.

4.2 Obstacle Length

Several paths, where the length l of the obstacle, *i.e.*, the size of the obstacle along the X -direction, is varied from 5 m to 20 m, are shown in Figure 5. The shapes of the paths, where the obstacle lengths are in the range 5–11 meters, are different from the shapes where the obstacle lengths are 15 and 20 meters. The difference corresponds to different extreme values of the vehicle orientation ψ around $X = 40$ m. The vehicle orientation for the first set of paths could be approximated with straight lines between extrema around $X = 20$ m and $X = 40$ m, but for the second set, there is a noticeable bend between these points, which also corresponds to a change in the steering direction for the corresponding segment.

For the considered optimization formulation, it is beneficial to immediately return to the original lane once the obstacle is passed. In all obtained maneuvers, the shape of the XY -path is such, that the vehicle touches the farthest corner of the obstacle. Information about the obstacle length in optimizations results in different optimal steering strategies and different velocity profiles (Figure 5) for $X > 20$ m.

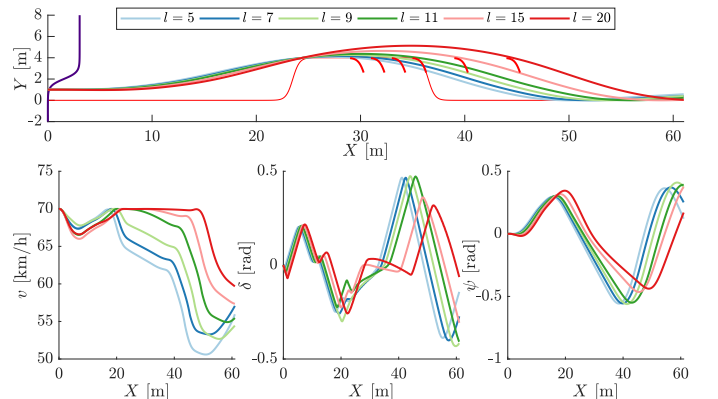


Figure 5: Paths and selected vehicle variables found for different lengths of the obstacle (in meters), with the initial velocity $v_0 = 70$ km/h. The same LDP objective is used. Red arcs show the farthest corner of the obstacle for different widths. All obstacles start at the same X coordinate.

4.3 Initial Velocity

Several maneuvers were computed with different initial velocities v_0 (see Figure 6). The velocity profiles for v_0 from 50 km/h

up to 70 km/h are almost equidistant from each other when plotted over X . This property could be used to predict an intermediate velocity profile for the range in between. The velocity profiles for $v_0 = 80$ km/h and $v_0 = 90$ km/h have a different behavior; the vehicle slows initially down more to be able to perform the maneuver.

For a relatively low initial velocity (50–60 km/h), the vehicle behavior is different compared to higher initial velocities; the vehicle first drives to the right relative to its direction of movement and then drives to the left to avoid the obstacle.

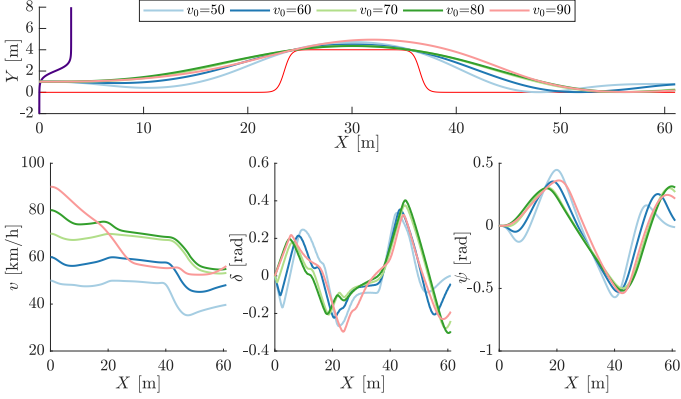


Figure 6: Paths and selected vehicle variables found for different initial velocities v_0 (km/h). The same LDP objective is used.

4.4 Distance to the Obstacle

Paths and selected variables for different initial distances to the obstacle are presented in Figure 7. The major parts of the shown state variables for different distances are very similar to each other, with some shift along the X -variable. Similarly to the results in Figure 6, the vehicle in Figure 7 steers opposite to the obstacle-avoidance direction in the beginning of the maneuver.

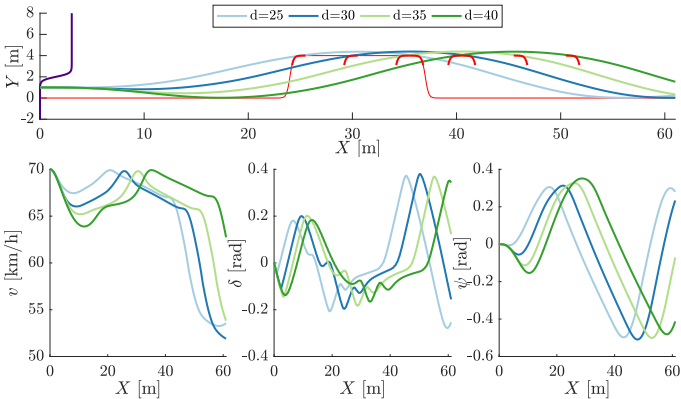


Figure 7: Paths and selected vehicle variables found for different obstacle distances (in meters), with the initial velocity $v_0 = 70$ km/h. The LDP objective is used. Red arcs show the top boundaries of the obstacle for different obstacle distances.

4.5 Maximum Steering Speed

One of the limiting factors for avoiding an obstacle at a given initial velocity is the steering dynamics of the vehicle steering servo. Lower bandwidth of the steering servo affects the steering strategies that are applicable in a certain scenario. Several trajectories were obtained for different values of the maximum steering rate, $\dot{\delta}_{\max}$. The resulting XY -paths are very similar, but with lower values of the objective function for higher allowed steering rates. Lower values of $\dot{\delta}_{\max}$ were limiting the pendulum-like steering behavior, noticeable by variations in the optimal steering and vehicle orientation before the obstacle.

4.6 Comments on Minimum Stopping Distance

In the case of a sudden obstacle appearance on the way of a car, there could be several different choices to try to cope with the situation. This paper mostly focuses on studying avoidance maneuvers by using the space in the opposing traffic lane. An alternative approach is to apply an emergency braking maneuver if possible.

For the considered setup, the minimum stopping distance varies from 9.7 m to 29.3 m for initial velocities in the range from $v_0 = 50$ km/h to $v_0 = 90$ km/h. For the highest velocity, the vehicle is not able to stop completely before the obstacle, decreasing the speed from 90 km/h to 42.3 km/h right before it. For $v_0 = 80$ km/h, the minimum stopping distance is 23.4 m, which means that the vehicle is able to completely stop before the obstacle, but results in an aggressive peak deceleration of about 11.8 m/s^2 . In practice, it could be a dangerous maneuver to perform, also because of the vehicles behind in the same lane. Considering uncertainties in the tire-road friction estimation and vehicle parameters, the total stopping distance could be significantly longer than estimated. For the same initial velocity, $v_0 = 80$ km/h, decrease in the distance would omit the possibility of a safe stop, but it is still possible to make an avoidance maneuver for the same initial velocity, as it is shown in Figure 8.

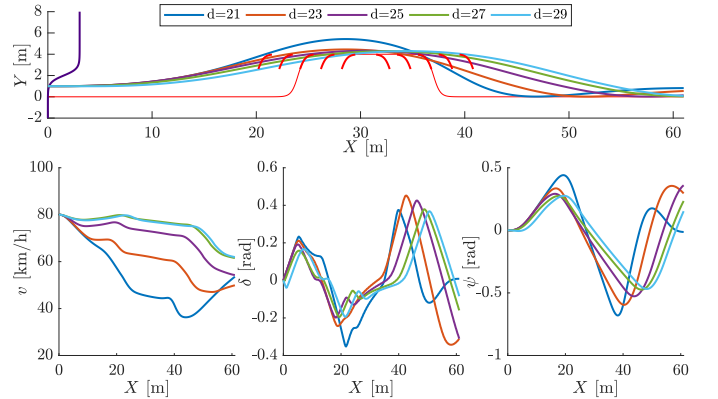


Figure 8: Paths and selected vehicle variables found for different obstacle distances (in meters), with the initial velocity $v_0 = 80$ km/h. The LDP objective is used. Red arcs show the top boundaries of the obstacle for different obstacle distances.

5 LDP COMPARISONS AND VARIATIONS

In this section, solutions to the considered problem using the LDP objective function are compared with solutions obtained using the minimum-time objective function. Several variations of the problem are considered to study the benefit of the observed pendulum-line behavior of the vehicle before the obstacle.

5.1 Comparison of Objective Functions

A comparison of the solutions to the optimization problem with the LDP objective function and minimum-time objective function is shown in Figures 9 and 10. Two variants of minimum-time optimization are considered: an minimum-time (MT) formulation with the same constraints as for the LDP case, which results in paths where the vehicle is comparably slower to return to the original lane (Figure 9), and an minimum-time with a top boundary (MTTB) formulation, where an additional lane-change boundary is added (the red dotted line in Figure 10), which is formulated as:

$$Y(t) \leq Y_{tb}$$

$$Y_{tb}(X(t)) = Y_{rw} - Y_{tbp}(1 - \tilde{H}_{X_{otu}}^{X_r}(X(t)) + \tilde{H}_{X_{otd}}^{X_r}(X(t))),$$

where Y_{tbp} is the road width and X_{otu} , X_{otd} are the points where the top boundary goes up and down, respectively. The values

of these parameters used in the optimization are 4, 12, and 47 meters, respectively.

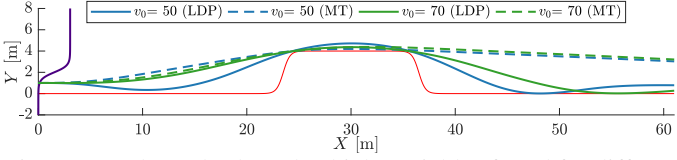


Figure 9: Paths and selected vehicle variables found for different initial velocities (km/h) and objectives (LDP and MT). The solid lines show the results for the LDP formulation and the dashed lines show the results for MT. The same constraints for all cases.

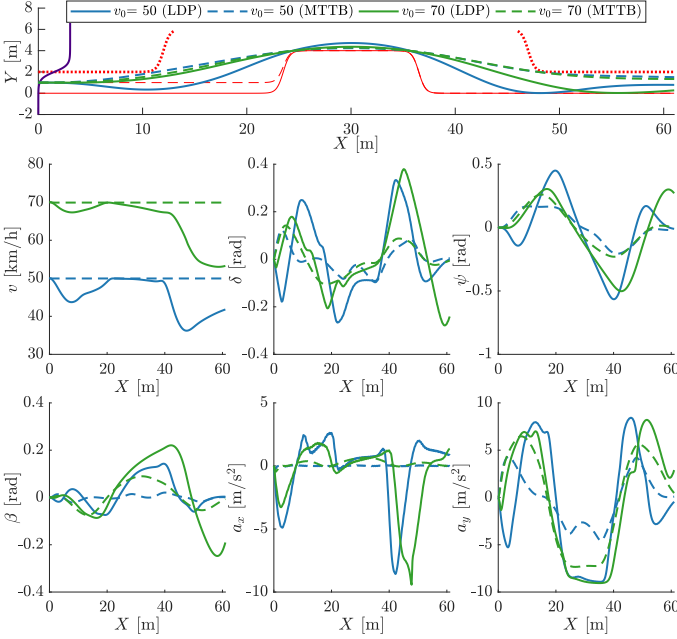


Figure 10: Paths and selected vehicle variables found for different initial velocities (km/h) and objectives (LDP and MTTB). The solid lines show the results for the LDP formulation and the dashed lines show the results for MTTB. The additional boundary in MTTB is shown as the red dotted line.

The tire-road friction admits the vehicle in MTTB optimizations to keep the maximum allowed velocity (which is equal to the initial velocity for the cases considered). However, in the MTTB case, the vehicle stays in the opposing lane for a longer time compared to the LDP optimization. Table 3 compares the time the vehicle is in the opposing lane and the maximum acceleration for a given optimization criterion and initial velocity. LDP optimizations give paths and trajectories that are safer in terms of the time that the vehicle stays outside its own lane. At the lower initial velocity, that difference is bigger (60%) than at the higher velocity (15%). Compared with MTTB optimizations, LDP optimizations result in higher changes in longitudinal a_x and lateral a_y accelerations, as well as bigger body-slip angle β (see Figure 10). The difference is caused by combination of the imposed speed limit (3) and the MTTB objective function (minimum-time), so the longitudinal component of the acceleration for MTTB trajectories is almost zero, resulting in lower values for the maximum acceleration (Table 3).

An alternative approach to formulate the objective function was evaluated by penalizing the integral squared-error norm (SEN) of lateral displacement that was used in [6] for the recovery part of the double lane-change maneuver. Here, it is applied for the full maneuver by using the following objective function:

$$\int_0^{t_f} (Y(t) - Y_0)^2 dt.$$

This function exhibits similar results compared to LDP optimizations in terms of trajectories (Figure 11), but the time in the

opposing lane is 12% and 2% longer for the low (50 km/h) and the high (70 km/h) velocity, respectively. Also, more aggressive braking after the obstacle is obtained, since the vehicle tries to return to the original lateral position, not just to its own lane. The lateral accelerations are very similar for LDP and SEN with differences for the area where $X = 30$ –40 m, where for the SEN optimization the vehicle steers more aggressively (δ in Figure 11) and for the slower velocity the slip angle is smaller for this part (dotted blue line in Figure 11).

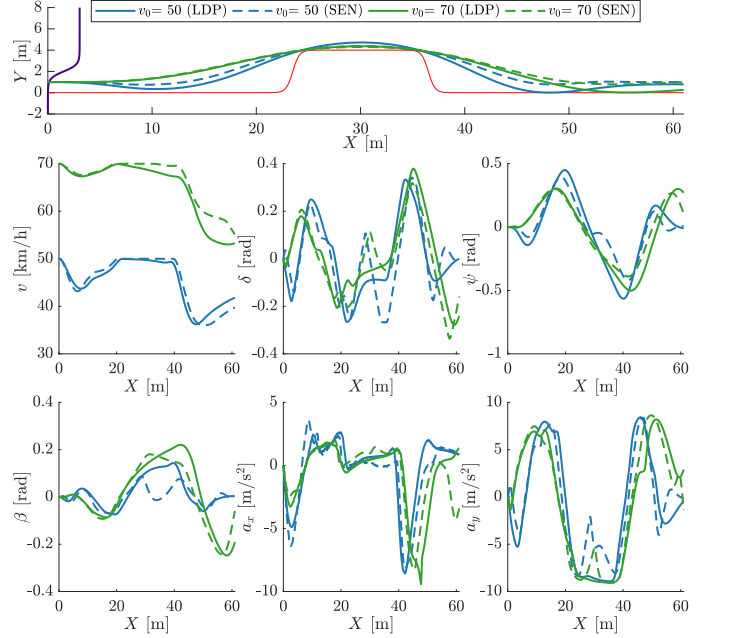


Figure 11: Paths and selected vehicle variables found for different initial velocities (km/h) and objectives (LDP and SEN). The solid lines show the results for the LDP formulation and the dashed lines show the results for SEN.

5.2 Pendulum-Like Behavior

At the beginning of the maneuver for the low velocities in the LDP optimizations, the vehicle steers in the opposite direction of obstacle avoidance (the vehicle orientation ψ and the steering angle of the maneuver δ decrease in Figure 10). This behavior might be counterintuitive, but it is optimal for the considered problem formulation. The scale of pendulum-like movements is limited by the width of the initial straight road considered in this double-lane change scenario. This scale is much smaller here than the scale of the pendulum-turn maneuver from racing driving experiments studied in [2].

Interesting to note is that even with a modification of the drivable area before the obstacle:

$$Y_{bb}^{\text{mod}}(X(t)) = 1 + (Y_{bbp} - 1) \tilde{H}_{X_{ou}}^{X_r}(X(t)) - Y_{bbp} \tilde{H}_{X_{od}}^{X_r}(X(t)),$$

such that the vehicle is unable to take the right side of its lane, it is still optimal to perform pendulum-like movements for the vehicle orientation and steering (Modv1 LDP in Figure 12).

Only when the minimum value of the steering variable δ is set to zero before the obstacle (the vehicle is unable to steer to the

Table 3: Time interval the vehicle is outside its own lane ($Y > Y_0$) and maximum acceleration for different initial velocities and objectives.

Name \ v_0	50 km/h		70 km/h	
LDP	1.64 s	9.6 m/s ²	1.57 s	10.0 m/s ²
MT	3.61 s	4.7 m/s ²	2.47 s	6.5 m/s ²
MTTB	2.66 s	4.6 m/s ²	1.80 s	7.4 m/s ²
SEN	1.85 s	9.3 m/s ²	1.60 s	9.3 m/s ²
Modv1 LDP	1.68 s	9.6 m/s ²	1.59 s	10.0 m/s ²
Modv2 LDP	1.69 s	9.7 m/s ²	1.57 s	10.0 m/s ²

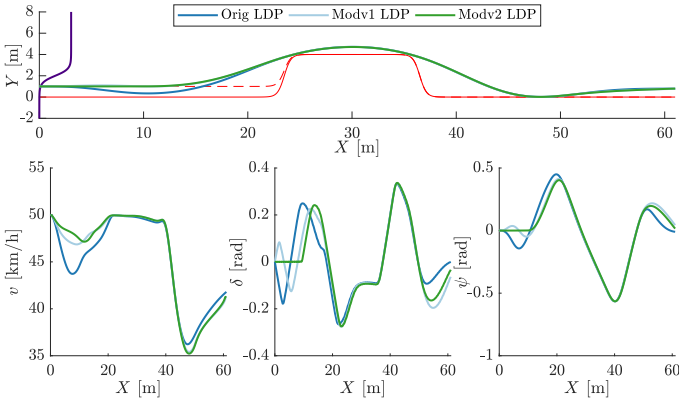


Figure 12: Paths and selected vehicle variables found for different modifications of the LDP problem formulation, with the initial velocity $v_0 = 50$ km/h. The red dashed line shows the modification of the bottom boundary, $Y_{bb}^{\text{mod}}(X(t))$, for Modv1 LDP.

right before the obstacle), the resulting optimal trajectory does not have the pendulum-like behavior (straight lines for δ and ψ initially for Modv2 LDP in Figure 12). The steering constraint is formulated as:

$$\delta \geq \delta_{\min}(X(t)),$$

where $\delta_{\min}(X(t))$ is defined as:

$$\delta_{\min}(X(t)) = -\delta_{\max} \tilde{H}_{X_{o\delta}}^{X_r}(X(t)),$$

where $X_{o\delta} = 15$ m.

The observed pendulum-like behavior allows the vehicle to stay in the opposing lane for a shorter time. When it is prohibited (Modv2 LDP in Table 3), the vehicle stays outside its lane 2.5% longer time, for the same initial velocity. For the high velocity, there is almost no difference, but such a pendulum-like behavior appears if a sufficiently long distance to the obstacle is available for the higher velocities (see Figure 7). The longer the distance, the more significant such behavior is, *i.e.*, if time allows it is advantageous to control the vehicle to achieve pendulum behavior.

6 DISCUSSION AND CONCLUSIONS

A lane-deviation penalty (LDP) motion-planning formulation was considered. It is based on a smooth approximation of the Heaviside step function, *i.e.*, the logistic function. The same single objective function is used to obtain the full maneuver, only constraints implied by the road and obstacle are needed.

The LDP maneuvers obtained for different parameter variations show that the paths and the state variables have many similarities for the different optimizations with LDP objective (*e.g.*, Figures 6 and 7). This property supports the idea of a maneuver-based online motion-planner for future development, where intermediate maneuvers are obtained by interpolation of the model inputs and simulation of the vehicle model.

Use of LDP also results in maneuvers with pendulum-like behavior before the obstacle. It is noticeable at low initial velocities (Figure 6) or longer obstacle distances (Figure 7), *i.e.*, if time to the obstacle permits. The scale of the maneuver is observed to be much smaller than in previous studies of the pendulum maneuver. The available time before the obstacle is one of the limiting factors for pendulum-like maneuvers to be feasible and optimal for the used formulation. Also the performance of the steering servo and the width of the obstacle (Figure 4) are limiting the application of the pendulum-like maneuvers. For the maneuver to be effective, there should be a drivable space available on the side of the vehicle opposite to the avoidance maneuver (Figure 12).

Results for the high initial velocity (Figure 5) and additional optimizations for the low initial velocity showed that the length

of the obstacle has no significant influence on the maneuver before the obstacle.

This paper studies evasive maneuvers, but it was also concluded that for the default version of the considered setup, $v_0 = 80$ km/h is the maximum initial velocity when it is still possible to fully stop before the obstacle.

No significant difference in computational complexity was observed between different optimization formulations since the total time of the maneuver is computed as part of the optimization in all cases.

Maneuvers from LDP-based optimizations, a minimum-time approach, and minimization of an integral squared-error norm from previous research were compared using an evaluation criterion (Table 3). The evaluation criterion was based on the consideration that the main danger in the double lane-change maneuver is proportional to the time a vehicle is forced to be in the opposing traffic lane. The LDP formulation allows to decrease this time. Lower initial velocities and longer distances to the obstacle give higher gains from LDP by employing pendulum-like maneuvers.

ACKNOWLEDGMENT

This work was partially supported by the Wallenberg AI, Autonomous Systems and Software Program (WASP) funded by the Knut and Alice Wallenberg Foundation.

REFERENCES

- [1] K. Berntorp, B. Olofsson, K. Lundahl, and L. Nielsen. "Models and methodology for optimal trajectory generation in safety-critical road-vehicle manoeuvres". In: *Vehicle System Dynamics* 52.10 (2014), pp. 1304–1332.
- [2] J. Yi, J. Li, J. Lu, and Z. Liu. "On the Stability and Agility of Aggressive Vehicle Maneuvers: A Pendulum-Turn Maneuver Example". In: *IEEE Transactions on Control Systems Technology* 20.3 (2012), pp. 663–676.
- [3] A. Arikere, D. Yang, M. Klomp, and M. Lidberg. "Integrated evasive manoeuvre assist for collision mitigation with oncoming vehicles". In: *Vehicle System Dynamics* (2018), pp. 1–27.
- [4] E. Frazzoli, M. A. Dahleh, and E. Feron. "Maneuver-based motion planning for nonlinear systems with symmetries". In: *IEEE Transactions on Robotics* 21.6 (2005), pp. 1077–1091.
- [5] ISO 3888-2:2011. *Passenger cars — Test track for a severe lane-change manoeuvre — Part 2: Obstacle avoidance*. International Organization for Standardization, Geneva, Switzerland, 2011.
- [6] P. Dingle and L. Guzzella. "Optimal emergency maneuvers on highways for passenger vehicles with two- and four-wheel active steering". In: *American Control Conf.* Baltimore, MD, USA, 2010, pp. 5374–5381.
- [7] J. Y. Wong. *Theory of Ground Vehicles*. Wiley, 2008.
- [8] H. Pacejka. *Tyre and vehicle dynamics*. Oxford, UK: Butterworth-Heinemann, 2006.
- [9] Modelica Association. <http://www.modelica.org>. (Date accessed: 30.04.2018).
- [10] A. Wächter and L. T. Biegler. "On the implementation of an interior-point filter line-search algorithm for large-scale nonlinear programming". In: *Mathematical Programming* 106.1 (2005), pp. 25–57.
- [11] HSL. *A collection of Fortran codes for large scale scientific computation*. <http://www.hsl.rl.ac.uk>. (Date accessed: 30.04.2018).